COMPARISON OF ELECTRON DENSITIES
MEASURED WITH LANGMUIR PROBES
AND WITH TWO DIFFERENT MICROWAVE DEVICES

H. M. J. KINDERDIJK and J. VAN ECK

Fysisch Laboratorium van de Rijksuniversiteit Utrecht, Nederland

Synopsis

Electron densities in the positive column of a low-pressure helium discharge are measured 1) with cylindrical and spherical Langmuir probes; 2) with a precision microwave interferometer and 3) with a microwave cavity. The resulting electron densities agree very closely for the two microwave diagnostics; the results obtained with the probes are about 30% lower. The origin of this difference is discussed. Electron mobilities are calculated from the measured electron densities and electric field. The agreement with theoretical and experimental results of other authors is good for results obtained at 0.5 torr; at lower pressures a gradually increasing difference is found.

1. *Introduction.* Electrical probes (Langmuir probes) are very useful in measuring the local electron density in plasmas. There is, however, still some doubt as to their quantitative results. We have compared the electron densities, obtained with spherical and cylindrical probes in the positive column of a helium discharge, with the results of a precision microwave interferometer and with microwave resonance cavities. The calculations necessary to determine the electron density from the phase shift (interferometer) and from the resonance-frequency shift (cavity) are given by Kinderdijk and Hagebeuk[1]) and by van Eck and Kinderdijk[2]).

The most important part of the interferometer is a circular waveguide enclosing the discharge tube over a length of 50 cm. So the electromagnetic waves are travelling along the discharge tube over an appreciable distance. This setup gives a high sensitivity and a simple geometry. As our results with the interferometer differed slightly from measurements with resonance cavities made by other investigators in the same types of discharges, we measured also the electron density with a resonance cavity oscillating in the TM_{010} mode. These measurements were performed simultaneously with the interferometer and the probes in the same discharge tube.

The electrical probe measures the density at a point, whereas the microwave devices measure an overall density. In order to compare the results from the microwave devices with those of the probes it is necessary to know the profile of the relative radial electron density in the discharge. This profile has been measured with spherical probes of 0.5 mm diameter which can be moved radially over the whole tube diameter (22 mm).

From the electron densities and the total discharge current we have calculated the electron drift velocity and subsequently the reduced electron mobility μp_0 in helium as a function of the quotient of field strength and pressure. These mobilities are compared with the results of other authors. Accurate measurements of field strength and gas pressure are then necessary as well as a good purification of the gas.

2. *Experimental procedure.* 2.1. Introduction. The measurements were performed in the positive column of a helium discharge. An overall view of the setup of three different devices, the Langmuir probes, the microwave interferometer and the microwave cavity, is given in fig. 1. A description of the different devices will be given below.

2.2. The discharge tube. The outer diameter of the discharge tube was 25 mm; its length was about 1 m. The tube consisted partly of pyrex and partly of quartz; the latter part was inserted for measurements with the microwave cavity.

Two flat probes (tungsten 1.5 mm diameter, separation in axial direction 680 mm) were mounted in the tube wall. Two cylindrical Langmuir probes of tungsten (length 3.0 mm, diameter 0.050 mm) were situated at the axis, and two spherical probes of platinum (diameter 0.50 mm) could be moved over the whole tube diameter. The construction enabled us to perform simultaneously measurements with the probes, the microwave cavity, and the interferometer. A barium-oxide-coated cathode and a molybdenum
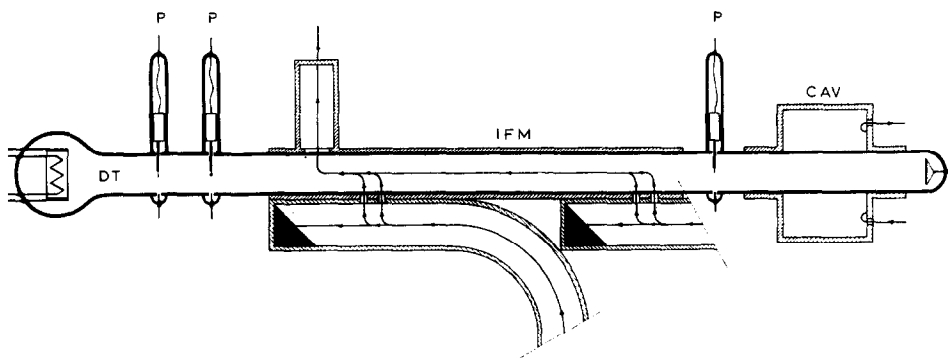

Fig. 1. The discharge tube (DT) with Langmuir probes (P) surrounded by the microwave interferometer (IFM) and the cavity (CAV).

anode were used. Preliminary measurements were performed in a discharge tube of 18 mm diameter which was used for a comparison of the results of probes and the microwave cavity.

The measurements were performed in the positive column of a helium discharge with pressures in the range of 0.1 to 1 torr; tube currents of 0.01 to 1 A were used. Nearly all the measurements were performed under such conditions that moving and standing striations were absent.

2.3. The vacuum system. The discharge tube was pumped by two oil diffusion pumps and one roughing pump in series. A water-cooled baffle and a bakeable liquid-nitrogen trap were used to keep down the creeping of the oil. The tube was disconnected from the pumping system by a Varian metal valve; a Granville Philips valve was used between the gas-inlet system and the tube. At a temperature of 450°C the whole glass system including the ionization gauges, the metal valves and the quartz diffusion tube was thoroughly degassed for about 24 hours. As a rule a residual gas pressure of about 5×10^{-10} torr (N_2 equivalent) was reached.

The helium gas (factory specification 99%) was introduced (and simultaneously purified) by diffusion through the wall of an auxiliary quartz tube. The gas pressure was measured with a special ionization gauge (Westinghouse[3]) type WL 7903). This ionization gauge was calibrated against a McLeod gauge. According to our test measurements the accuracy was about 5% over the pressure range of 5×10^{-2} to 1 torr.

2.4. Probe circuits. The electron density n_e and the electron temperature T_e were determined with the help of a current–voltage characteristic of a probe (fig. 3, curve a). Different electric circuits were used for the determination of the current–voltage characteristic (probe curve) of the Langmuir probes. The majority of the results were obtained with the system shown in fig. 2.

The probe curve was obtained on the screen of an oscilloscope and photographed (see fig. 2). A 50 V sweep was applied to the probe. The probe current was measured over a resistor R which was variable from 30 to 1000 Ω, so that the same sensitivity (50 mV/div) of the vertical deflection of the scope could be used in all cases. The effect of the voltage loss over the resistor R was eliminated by measuring the probe voltage directly on the probe (*via* a 100 MΩ resistance). Sweeping times as short as 1 ms for the whole curve were used without influencing the probe characteristic, as could be proved by taking data at somewhat shorter and longer sweeping times.

A 0.1 ms sweep did give a slightly deformed characteristic. In each exposure (exposure time 100 ms) many coinciding traces were photographed. The photographs were enlarged for the evaluation of the data.

The correct interpretation of a probe curve depends largely upon the determination of the position of the "knee" (K in fig. 3) in the curve,
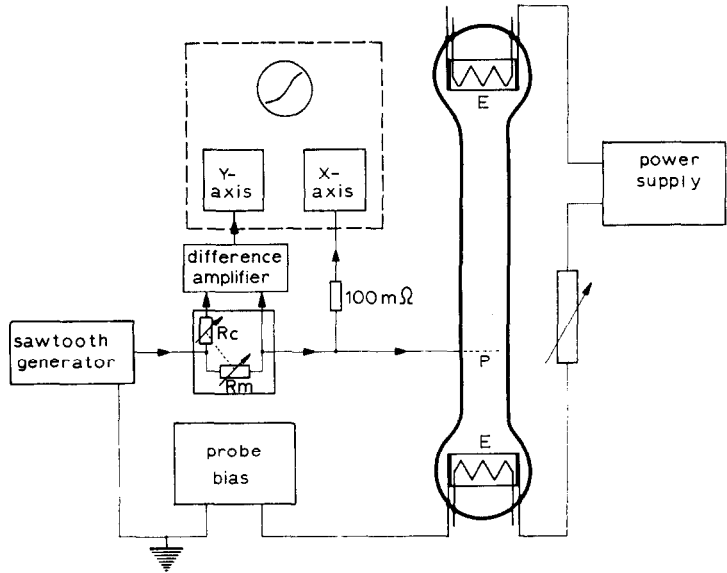
Fig. 2. Measuring system for fast probe measurements. The voltage of the probe (P) is varied by the sawtooth generator; the resulting current–voltage characteristic is recorded with the help of the oscilloscope. The discharge current between the electrodes (E) is fed by the power supply.
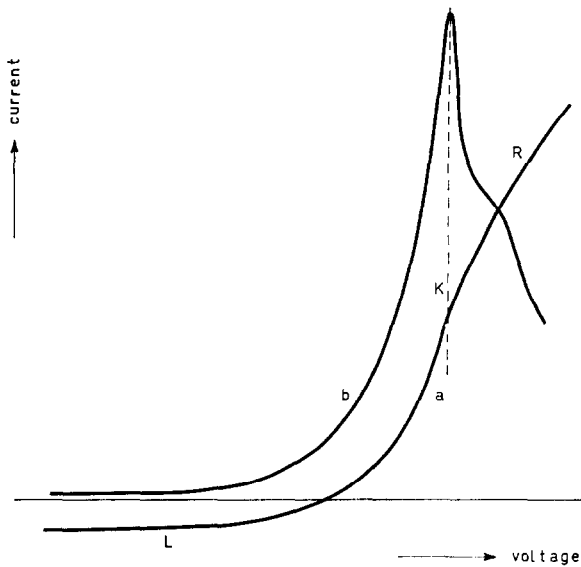

Fig. 3. The current–voltage characteristic of a probe (a) and its first derivative (b). The peak of the first derivative curve coincides with the knee (K) of the probe characteristic, which separates the positive part (R) and the negative part (L) of the curve.
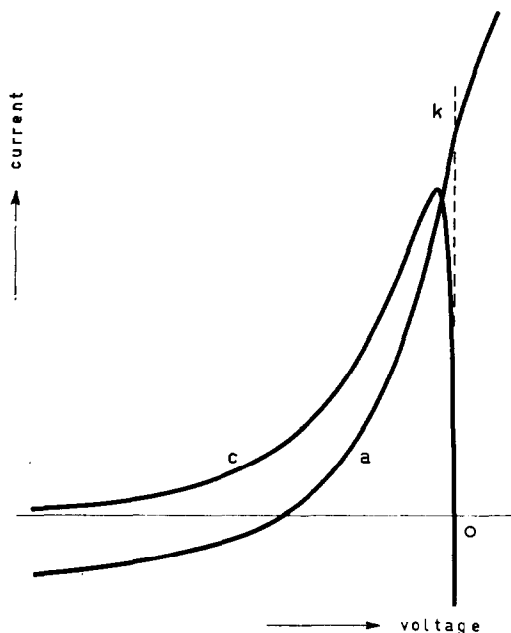
Fig. 4. Example of a probe curve (a) and its second derivative (c). The zero crossing of the second derivative curve (O) determines the knee (K) in the probe characteristic.

where the probe has the same potential as the local plasma. From the electron current at this potential (determined by the "knee") the electron density can be calculated if the average velocity of the electrons is known. In a latter stage of the investigations the probe curve was therefore differentiated by means of an operational amplifier. From the maximum in the first-derivative curve the "knee" was easily found. A few measurements were performed with the help of a circuit by which the probe curve and its second derivative were recorded by means of an $X-Y$ plotter (see fig. 4). An extensive description of this device has been given by Luyendijk and Van Eck[4]. An objective determination of the space potential ("knee" in the probe curve) is again possible; this time from the zero crossing of the second-derivative curve. The second-derivative curve of the current–voltage characteristic is directly related to the velocity distribution of the electrons.

2.5. The microwave interferometer. The circuit of the microwave interferometer is given in fig. 5. The microwaves ($f = 9.06$ GHz) from the klystron were coupled to the waveguide around the discharge tube at two places (331 mm apart) by two pairs of coupling holes. Backward waves were suppressed by using $\frac{1}{4}\lambda$ distance between the holes of each pair, which was facilitated by the adaptable input frequency. The interferometer had
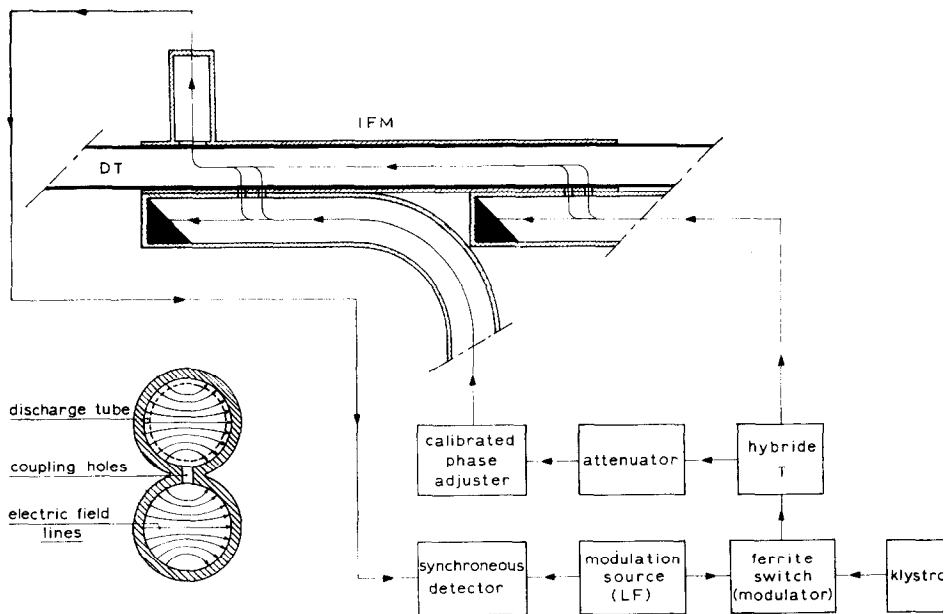
Fig. 5. The measuring circuit of the microwave interferometer (IFM) with the dis-
charge tube (DT).

Fig. 6. The measuring circuit of the microwave cavity (CAV) with the discharge
tube (DT).

a high sensitivity because the electromagnetic waves propagated over a
long distance through the discharge. Reflections of the electromagnetic
waves at the glass wall were eliminated as the coupling holes were drilled
at places where the electric field of the TE_{11} mode was always zero. The
microwaves were produced by a powerful Varian V-50 klystron. This was
necessary as the coupling degree of the e.m. waves into the discharge tube

was rather low (−20 dB). The microwaves were chopped by a Ferrotex ferrite switch which was controlled by a 1 kHz modulation scource and then fed into the branches of the interferometer by a hybride T. From both branches the waves were coupled into the circular waveguide, which contained the discharge tube. Using a synchronous detector for sensitive zero indication, we adjusted the calibrated phase shifter, until the outcoming signal had reached its minimum. The phase shift, caused by the electron density in the discharge, was found directly from two readings.

2.6. The microwave cavity. The circuit of the microwave cavity is given in fig. 6. The diameter of the cylinder was 75 mm and the length 50 mm. The discharge tubes could be introduced through the coaxial end holes of 25 mm diameter. The cylindrical microwave cavity was used in the TM_{010} mode (resonance frequency about 3 GHz). Signals from a 2–4 GHz sweep oscillator were coupled into the resonance cavity and into a direct-reading frequency meter (calibrated cavity). The rectified signals of both cavities were subtracted by a differential unit of an oscilloscope. The time base of the oscilloscope (sawtooth voltage) also controlled the sweeping time of the sweep oscillator. From the display on the screen it was seen whether both cavities had the same resonance frequency. The value was then read from the calibrated cavity. The electrons of the discharge caused a shift of the resonance frequency which was found from two readings of the resonance frequency: with and without the discharge. The electron density was then calculated from this frequency difference.

3. *Theory and interpretation of probe measurements.* 3.1. Introduction. Langmuir[5]) has given the first complete picture of the interpretation of a current–voltage characteristic of a probe (spherical, cylindrical or flat). The theory was developed assuming a maxwellian electron velocity distribution. In a low-pressure and low-current gas discharge, however, the electron velocity distribution is generally not maxwellian. A low-pressure helium discharge is an exception to this rule; a maxwellian energy distribution is found up to about 17 eV. Theoretical calculations of the electron velocity distribution performed by Postma[6]) confirm these conclusions.

3.2. Analysis of the probe characteristic. The probe measurements were performed with Langmuir probes. The electron density and average electron velocity at the axis of the tube were measured with cylindrical probes of tungsten (length 3.0 mm, diameter 0.050 mm) and with spherical probes of platinum (0.50 mm diameter). The radial electron density profiles were measured with the spherical probes which were moved over the whole tube diameter. Pictures of probe curves with first and second derivatives are given in figs. 3 and 4.

The electron current from a uniform plasma to a probe with a retarding

voltage $-V$ is given by:

$$i^-(V) = \tfrac{1}{4} S n_e e \left(\frac{2}{m}\right)^{\frac{1}{2}} \int\limits_{eV}^{\infty} U^{\frac{1}{2}} \left(1 - \frac{eV}{U}\right) g(U) \, \mathrm{d}U, \tag{1}$$

where S is the area of the probe surface if it is a convex probe, $U = \tfrac{1}{2}mv^2$ is the kinetic energy of the electrons in the undisturbed plasma and $g(U) \, \mathrm{d}U$ is the fraction of the electrons with energy between U and $U + \mathrm{d}U$. For a maxwellian distribution $g(U) = 2\pi^{-\frac{1}{2}}(kT_e)^{-\frac{3}{2}} U^{\frac{1}{2}} \exp(-U/kT_e)$.

The validity of expression (1) has been demonstrated by Medicus for the flat probe and for the spherical probe[7]. He uses the fact that a mono-energetic and isotropic velocity distribution with electron density n_ν and velocity v_ν will give the same current on a spherical probe as a mono-energetic beam with current density $j_\nu = n_\nu v_\nu \lambda$. For such a beam the ef-fective cross section of the probe (for electron capture) is

$$\sigma_\nu(U_\nu, V) = \tfrac{1}{4} S \left(1 - \frac{eV}{U_\nu}\right)$$

if $\tfrac{1}{2}mv_\nu^2 = U_\nu$, and V is the retarding voltage of the probe. He divided an arbitrary isotropic velocity distribution in monoenergetic swarms with ener-gies $U_1, U_2, U_3, \ldots, U_\nu, \ldots$, and found that the corresponding probe currents $i_1^-, i_2^-, \ldots, i_\nu^-, \ldots$, were given by:

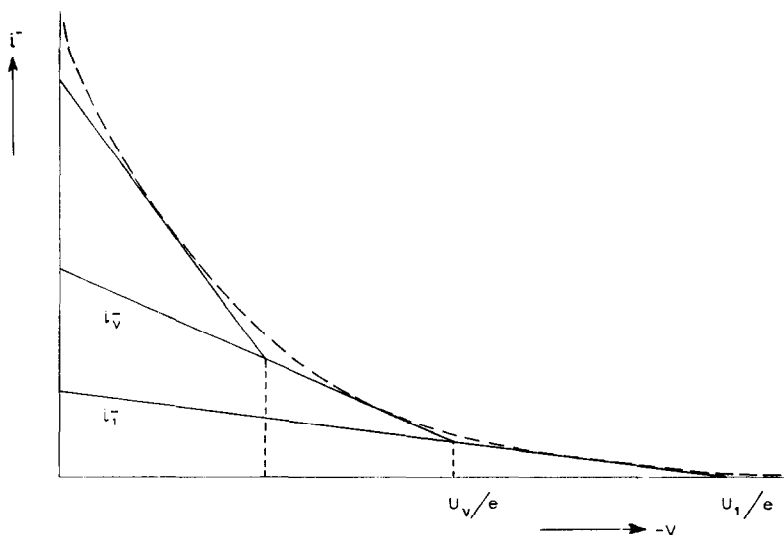$$i_\nu^- = \tfrac{1}{4} S n_\nu e v_\nu (1 - eV/U_\nu). \tag{2}$$

Fig. 7. The total electron current $i^-(U/e)$ to a negative probe formed by a summation of monoenergetic swarms with energies U_ν and corresponding probe currents i_ν^-.

According to expression (2) each swarm produces a contribution to the probe current that rises linearly from zero at $eV = U_v$ to $\frac{1}{4}Sn_eev_v$ at $V = 0$. The total probe current i^- is found by an integration of these subcurrents (see fig. 7).

Kagan and Perel[8]) have pointed out that expression (1) can be used for any convex probe in a plasma with an isotropic velocity distribution. They argue that according to the Liouville theorem the electron distribution does not change along a particle trajectory if there are no collisions. This means that the behaviour of each electron can be found from the collisionless Boltzmann equation[9]). The electron energy distribution at the probe surface (p) is then found from the electron energy distribution of the undisturbed plasma (0) by the substitution $U_p - eV_p = U_0$. By an integration over the contributions to the probe current from the electrons with an inward velocity component, they find expression (1), which for a maxwellian energy distribution reduces to:

$$i^-(V) = \tfrac{1}{4}Sn_ee(8kT_e/\pi m_e)^{\frac{1}{2}} \exp(-eV/kT_e). \tag{3}$$

From this relation it is easy to derive the well known relation:

$$n_e = 4.03 \times 10^{16} i_0^- S^{-1} T_e^{-\frac{1}{2}}, \tag{4}$$

where S is the area of the probe in m^2, i_0^- the electron current to the probe in A when it is at space potential, and T_e the electron temperature in K.

For the calculation of this electron density we need to know the electron temperature and the current i_0^- at space potential.

3.2.1. The electron temperature. The electron temperature can be found in different ways. The most complete method (I) to investigate the problem of the electron temperature or the average electron velocity is to measure the electron energy distribution. The electron energy distribution can be determined from the second derivative (SD) of the current–voltage curve of the probe (see fig. 4). This method has been discussed by Luijendijk and Van Eck[4]), who also give results of measurements in a helium discharge. They found a maxwellian velocity distribution up to an energy of about 17 eV (the SD curve gives a straight line in semi-log plot). This result is confirmed by our measurements and it is in agreement with the calculations of Postma[6]). At higher energies a line with a steeper slope is found in the semi-log plot, indicating a deficiency of electrons at higher energies. This is also in agreement with the theoretical calculations involving the effects of inelastic collisions (excitation and ionization of the atoms). By another method (II) the electron temperatures are found directly from the negative part of the probe characteristic by plotting the logarithm of the electron current *versus* the probe voltage. For a maxwellian velocity distribution of the electrons one expects a straight line. The slope of this line gives

then the electron temperature. In our case we could produce a nearly straight line in such a plot by adding a constant value (see 3.2.2) to the measured probe current. The temperatures derived in this way are in agreement with the results of the SD apparatus. Since the SD automatically neglects currents which are constant or linear in V, one should expect (after a proper correction) from both methods the same results for the electron temperature.

As the SD current is extremely small the discharge must be quiet during the recording of a probe characteristic (about two minutes). Our measurements were spread over a broad range of discharge currents and gas pressures. Accordingly a large number of electron-temperature determinations were needed. Therefore the faster method (II) originally introduced by Langmuir[5]) was used for the interpretation of our measurements.

3.2.2. The random electron current. The value of i_0^- can be determined from the "knee" (K in fig. 3) in the probe characteristic or from the shape[10]) of the probe characteristic for a positive probe (part R in fig. 3). Both methods were used. For a precise determination of the knee in the probe curve which normally is rather laborious, the first-derivative or (in a few cases) the second-derivative curve (SD) was used. The measured probe current, however, must be corrected for electrons ejected by metastable atoms and reflected electrons. A short survey of these sources of errors will be given:

a) *The ejection of electrons by metastable atoms* will be caused by He atoms in the 2^3S and 2^1S state. Mewe[11]) has calculated recently the population of these levels for a simplified model of a gas discharge. He also gives an estimation of the ejection current i^*. If η is the efficiency of the electron ejection by metastable atoms from the probe surface it can easily be calculated that

$$i^* = i_0^- \, \eta(n^*/n_e)(T_g m_e/T_e m_i)^{\frac{1}{2}} = 0.0117 \, i_0 \, \eta(n^*/n_e)(T_g/T_e)^{\frac{1}{2}}, \tag{5}$$

where T_g is the temperature of the atoms, m_i the mass of the atoms or ions and n^* the metastable-atom concentration. The ejection current will be of the order of the ion current if $\eta(n^*/n) \times (T_g/T_e)^{\frac{1}{2}} \approx 1$. Using the values of n^* given by Mewe, we calculate that for our experimental conditions i^* varies between 5 and 10% of i_0^-.

b) *The ejection of electrons by photon impact* on the probe surface gives a negligible current density. The main source is the 2^1P-1^1S transition (584 Å) which is strongly absorbed in the used pressure range. Extrapolating the results of Dorrestein[12]) to the higher pressures of our gas discharge a contribution below $10^{-4} \, i_0^-$ is found. A rough calculation using the absolute cross sections and escape factors as given by Mewe[11]) gives the same order of magnitude.

c) *The ion current* is neglected as

$$i_0^+ = i_0^- (T_i m_e / T_e m_e)^{\frac{1}{2}} \approx 10^{-3} i_0^- .$$

d) *Secondary emission and reflection by electrons* will noticeably influence the results. A substantial fraction of the electrons that fall on the probe surface is reflected. Hölzl[13] measured the reflection coefficient, δ, for normal incidence on clean platinum as a function of the energy. The fraction which is elastically reflected was about 10%. He found that the true secondary emission increased linearly from zero at 2 eV upto 30% at 20 eV. Approximating the sum of the reflection and secondary-emission coefficient by $\delta(U_e) = 0.02 \times V$, and assuming $\delta(U_e)$ to be independent of the angle of incidence, we find for a maxwellian distribution:

$$\delta(T_e) = 0.03 \times (kT_e/e),$$

so that for $kT_e/e = 8$ V a reflection and secondary-emission coefficient of 24% is found for a clean surface of platinum. According to measurements of Ahearn[14] we expect about the same values of $\delta(T_e)$ for tungsten in the low-energy region.

e) *Incomplete maxwellian energy distribution.* Using expression (4) we find a value for the density, which is only correct in the case of a complete maxwellian energy distribution. The shortage of fast electrons for the discharge in helium makes the validity of expression (4) disputable; a correction factor should be applied to electron densities which are calculated with the help of expression (4). Such a correction is easily found for a maxwellian distribution that has been cut off at 20 eV.

The new distribution has the normalizing constant

$$C = \int_0^{20e/kT_e} x^{\frac{1}{2}} e^{-x} dx \Big/ \int_0^{\infty} x^{\frac{1}{2}} e^{-x} dx. \tag{6a}$$

The random current at space potential from the cutoff distribution, i_0^- cut, is compared to the random current from a maxwellian distribution with the same temperature. Their ratio is:

$$F = i_0^- \text{ cut}/i_0^- \text{ maxw.} = \frac{1}{C} \int_0^{20e/kT_e} x e^{-x} dx \Big/ \int_0^{\infty} x e^{-x} dx. \tag{6b}$$

Values of F are given in table I.

The energy distribution is not abruptly cut off at 20 eV, but the electron density as a function of energy begins to diminish more than would correspond to a maxwellian distribution at about 17 eV. The calculated values of the correction factor F will therefore give only a rough estimation.

3.2.3. Positive-probe characteristics. The electron density can also

The quotient F^{-1} of the random currents from a maxwellian energy distribution of temperature T_e and its cutoff distribution. To get the cutoff distribution, the complete maxwellian distribution is cut off at eV_{exc} and normalized again.

eV_{exc}/kT_e	1	2	3	4	5	6
F^{-1}	1.64	1.25	1.11	1.06	1.02	1.01

be found from the shape of the positive part of the probe characteristic[10]. We used this method sometimes for the analysis of photographed characteristics. The slower registered curves, from the $X-Y$ recorder, cannot be used as they are influenced by the heating up of the probe at positive voltages. Moreover, in such cases sometimes the positive probe was destroyed by arcing. Verwey[15] used a special method to eliminate these effects; as a consequence he could measure characteristics of very thin wire probes.

Another feature of the positive probe is the recapture of secondary electrons. True secondary electrons which have energies below 0.2 eV cannot escape and a part of the reflected electrons will also be recaptured because of their energy losses.

We compared values of electron densities calculated from the positive-probe characteristic with results from the current at plasma potential. From the positive probe we found for a tungsten-wire probe of 50 μ diameter about 10% higher values. When we included the space-charge corrections as given by Van Eck and Kinderdijk[16] the difference between the two methods diminished to 5% (see also section 6.2).

3.4. Radial density profiles. In order to determine the average electron density over the tube cross section the radial profile of the electron density was measured with spherical probes of platinum that were moved over the whole tube diameter. These probes (0.50 mm diameter) were better suited to measure the local electron densities than the cylindrical probes.

As the densities near the wall were quite low, it was difficult to determine the space potential there. Therefore the electron densities were derived from the slopes of the probe characteristic at a certain potential above space potential. A summary of this method, which is an application of the similarity rules, is given in ref. 16.

In order to check this method we compared these electron densities to the results calculated from the current at space potential, which was found with an SD apparatus. These measurements were performed in a broad tube (50 mm diameter) with a helium pressure of 0.25 torr and a discharge current of 0.3 A. The radial profile was measured and the results of the comparison are given in table II which shows a reasonable agreement.

<div align="center">TABLE II</div>

The relative electron density $n_e(r)/n_e(0)$ as a function of the distance from the tube axis determined with the aid of the slope and the knee of the probe curve.
Discharge data: $R = 25$ mm; $p = 0.25$ torr; $I = 0.3$ A.
Probe data: platinum sphere; 0.70 mm diameter.

r/R	0.0	0.2	0.4	0.6	0.8	1.0
$n_e(r)/n_e(0)$						
From the slope	1.0	0.92	0.82	0.58	0.34	0.05
From the knee	1.0	0.95	0.79	0.57	0.31	0.08

By means of the "slope" method a broad range of pressures and currents was covered which gave more or less the same electron-density profiles. Two examples are shown in fig. 8 together with a Bessel function and a parabola. The measured profiles are rather sharp and have a good symmetry as was verified in the small and in the broad tube. In fact the results given in fig. 8 were taken over the whole tube diameter. The profiles are approximated by a zero-order Bessel function with 10% of its top value at the wall: $n_e(r)/n_e(0) = J_0(2.22r/R)$; and for comparison by a parabola: $n_e(r)/n(0) = 1 - r^2/R^2$. The Bessel function gives a better fit, resulting in an average density of $0.50 \pm 0.5\%$. The average density of the measured
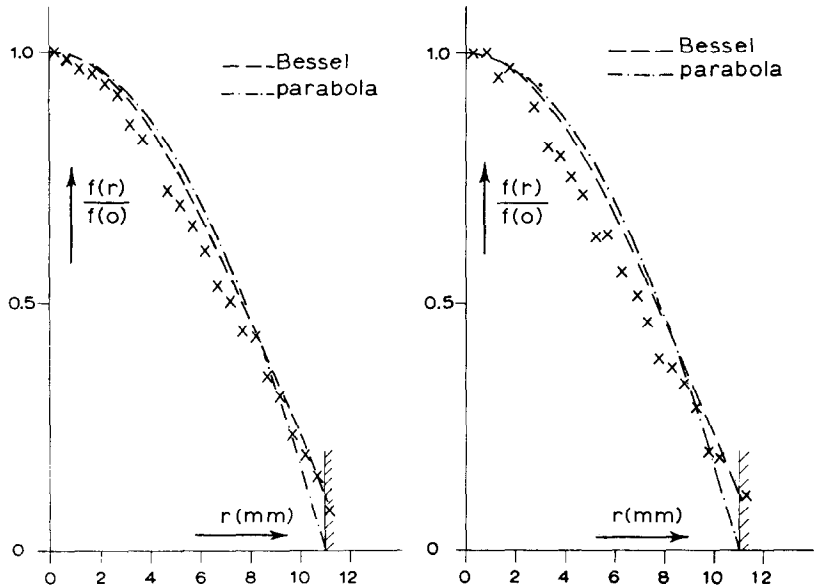

Fig. 8. Radial profile of the electron density (crosses) measured with the help of a spherical probe (0.50 mm diameter) compared to a Bessel function and a parabola. a) Tube current 23 mA; pressure 0.11 torr. b) Tube current 76 mA; pressure 0.80 torr.

profiles is about $0.45n(0)$ in good accordance with a Bessel function with zero density at the wall (see Bessel A, table IV).

4. *The microwave interferometer.* 4.1. Interpretation of the measured phase shifts. In a wave guide of effective length L, the phase shift, $L\Delta\beta$, which is due to the introduction of a dielectric material or a plasma, is interpreted with the help of the calculations given in ref. 1.

For a waveguide homogeneously filled with plasma (without a glass tube), the relation between the plasma radial frequency ω_p and the propagation constant β is given by expression (26) of ref. 1.

$$\omega_p^2/\omega^2 = 1 - \varepsilon_p = (\beta_0^2 c^2/\omega^2 - \beta^2 c^2/\omega^2), \tag{7}$$

where ω is the klystron frequency, ε_p the dielectric constant of the plasma, c the light velocity in vacuum and β_0 is the propagation constant in the empty waveguide. In our case $\beta_0 = 118.02$ rad/m.

It was not possible to derive a similar relation for a plasma in a glass tube in a mathematically closed form. However, the results of the numerical calculations (given in ref. 1) can be approximated for our experimental circumstances by:

$$\omega_p^2/\omega^2 = 1 - \varepsilon_p = K(\beta_g^2 c^2/\omega^2 - \beta^2 c^2/\omega^2), \tag{8a}$$

for the homogeneous case, and by

$$\langle \omega_p^2/\omega^2 \rangle = K(\beta_g^2 c^2/\omega^2 - \beta^2 c^2/\omega^2), \tag{8b}$$

for an inhomogeneous plasma with a parabolic radial profile of the electron density. Here $\langle \omega_p^2/\omega^2 \rangle$ is averaged over the cross section of the tube and β_g is the propagation constant with the glass tube only. Values of the factor K can be derived from ref. 1: tables I (homogeneous case) and III (inhomogeneous case). They depend on the assumed radial profile of the electron density and slightly on the dielectric constant and the thickness of the wall of the discharge tube. For a homogeneous plasma in a pyrex tube with inner radius $a_i = 11.0$ mm, outer radius $a = 12.5$ mm, and the dielectric constant of the glass $\varepsilon_{glass} = 5$ we find $K = 0.92$ (ref. 1, $a_i/a = 0.88$). For the plasma with a parabolic radial density profile in the same tube we find $K = 0.78$. After substitution of $\omega_p^2 = n_e e^2/\varepsilon_0 m_e$ [ref. 1, expression (1)], and $\omega/2\pi = f = 9.006$ GHz, the expression (8b) becomes for this discharge tube:

$$\langle n_e \rangle \text{ m}^{-3} = 2.21 \times 10^{13}(\beta_g^2 - \beta^2) \text{ rad}^2 \text{ m}^{-2}, \tag{9}$$

or

$$\langle n_e \rangle \text{ m}^{-3} = 6.00 \times 10^{15} \Delta\beta(1 - \Delta\beta/2\beta) \text{ rad m}^{-1}, \tag{10}$$

where $\langle n_e \rangle$ is the average electron density in the tube and $\beta_g = 135.8 \text{ rad/m}$ for the empty tube and $\Delta\beta = \beta_g - \beta$.

4.2. Calibration. We checked the above-mentioned calculations using media with known dielectric constants. This verification was necessary since reflections of the microwaves at the coupling holes and other unknown effects might be possible.

An empty pyrex tube ($\varepsilon_g = 4.5$), with inner and outer diameters equal to 20.1 and 24.8 mm, respectively, was put in the waveguide. The calculated shift was $154.4 - 118.0 = 36.4 \text{ rad/m}$ for this tube thickness. The measured shift was also 36.4 rad/m, in agreement with the calculations.

TABLE III

Phase shifts $\Delta\beta$ and specific weights ρ of polystyrene balls in glass tubes with inner diameter a_1 and outer diameter a. ($a \approx 25$ mm). From $\langle a_1/a \rangle = 0.868$ it follows that $K = 0.914$.

a_1/a	$\Delta\beta$ (degrees)	$\rho \times 10^6$ kg/m^3
0.870	61	192
0.860	57	187
0.860	56	188
0.875	61	193
0.875	62	194
0.865	56	183
$\langle a_1/a \rangle = 0.868$	$\langle \Delta\beta \rangle = 59 \pm 2\%$	$\langle \rho \rangle = 196 \pm 2\%$

Some other glass tubes were filled with small balls of polystyrene foam. The dielectric constant is then dependent upon the average density in the tube. This density was determined by measuring the tube volume v and the total weight w of the foam balls in each case. With the help of expression (8a) the value of $\varepsilon - 1$ was calculated from the measured phase shift. The results are given in table III. With $K = 0.914$ (see table I of ref. 1; the value of K was interpolated) and $\beta_g = 136$ the value of $(v/w)(\varepsilon - 1) = 1.12 \times 10^{-2} \text{ m}^3/\text{kg} \pm 5\%$ at 9 GHz was found.

The dielectric constant of the foam balls was measured separately with the closed cavity (appendix I). From four independent measurements we calculated: $(v/w)(\varepsilon - 1) = 1.08 \times 10^{-2} \text{ m}^3/\text{kg} \pm 2\%$ at 3 GHz. The difference of about 4% with the interferometer is within the error range though perhaps there is a small frequency effect. We verified that turning the tube around its axis gave no significant variation to the results. In conclusion we may say that the calculations and measurements are in good agreement with each other.

4.3. Radial profile. The calculations in ref. 1 were performed as-

TABLE IV

Calculated propagation constants β for different profiles; $\langle \omega_p^2/\omega^2 \rangle = 0.0843$

Profile	β rad/m	$\Delta\beta$ rad/m
Empty	135.86	—
Homogeneous	129.73	6.13
Parabolic	128.65	7.21
Bessel A	128.46	7.40
Bessel B	128.69	7.17

suming a parabolic profile of the electron density with zero density at the wall. As was verified by us (section 3.4) the profile is somewhat better approximated by a Bessel function which has zero density at the wall (Bessel A). The results for $\Delta\beta$ in this case, which are given in table IV, differ about 3% with those of a parabola profile. A Bessel function with 10% of its top value at the wall (Bessel B) gives a difference of 0.6% with the parabola. As a consequence we performed all the calculations with a parabola profile because this is easier and the difference with "Bessel A" is only 3% in a representative case.

5. *The microwave resonance cavity.* 5.1. Calibration procedure. The use of the microwave cavity is based on the measurement of the shift in the resonance frequency caused by the introduction of a dielectric material or a plasma in the cavity. The connection between the frequency shift and the average plasma density of a radially non-uniform plasma was calculated by us (ref. 2) for a closed cylindrical cavity. For an "open cavity" (a cavity with two coaxial end holes) the results are not very different but the problem was more difficult and was not solved numerically. As the measurements were performed in an open cavity, a quantitative relation connecting the frequency shift in the open cavity to that of the closed cavity must be found before the calculations given in ref. 2 could be applied. This relation was found empirically by comparing the frequency shifts in two situations: a) the (measured) frequency shift due to the introduction of a rod with known dielectric constant and diameter in a long quartz tube around which the open cavity had been mounted; b) the (calculated) frequency shift for this rod in a closed cavity with quartz tube, where rod and tube are of the same length as the cavity.

In fact these comparisons were made for a number of rods with different diameters and of different dielectric materials. Among others rods of foamed polystyrene were used, because in this case an $\varepsilon \approx 1$ could be obtained, which has approximately the same value as is given by a gas discharge. In this calibration two different quartz tubes were used, with inner and

outer diameters of 15 and 17.1 mm for one tube, and 21 and 24.6 mm for the other one. The accurate values of the dielectric constant ε of the different materials used for the calibration, were measured separately with the closed cavity; see appendix I.

Values of the measured frequency shift (situation a) and values of the calculated shift (situation b) are given in table V. Their quotient, γ, is nearly a constant, approximately independent of the dielectric materials and the diameters of the quartz tubes, as expected; the average value of γ is 0.86.

Thomassen[17] has tried to calculate roughly the influence of the end

TABLE V

Comparison of frequency shifts with open and closed end holes;
$\gamma = \Delta f$ open/Δf closed

Dielectric material	Diameter (mm)	Inner–outer diameter quartz tube in mm	Δf (MHz) open	Δf (MHz) closed	γ
Teflon	5.15	15.1–17.1	21.5	26	0.83
,,	4.76	,, ,,	18.5	22	0.84
Parafine	12.4	,, ,,	142.7	168	0.85
,,	9.65	,, ,,	90.2	106	0.85
Teflon	12.25	,, ,,	117	135	0.85
					$\langle \gamma_1 \rangle = 0.84$
Styrofoam	14.6	15.2–17.1	5.8	6.8	0.86
		,, ,,	5.8	6.65	0.88
		,, ,,	6.2	7.2	0.86
		,, ,,	6.6	7.6	0.87
					$\langle \gamma_2 \rangle = 0.87$
Styrofoam	21.6	21.8–24.8	9.0	11.3	0.80
		,, ,,	9.4	10.6	0.89
		,, ,,	9.9	11.0	0.90
		,, ,,	9.8	11.4	0.86
					$\langle \gamma_3 \rangle = 0.86$

$\langle \gamma \rangle = \frac{1}{3}(\langle \gamma_1 \rangle + \langle \gamma_2 \rangle + \langle \gamma_3 \rangle) = 0.86$

holes on the frequency shift. From his calculations we can derive for our case a value of 0.9 for the reduction factor γ, in agreement with our results.

5.2. Determination of the electron density. Our interpretation of the frequency shift of the cavity due to the introduction of a gas discharge in the quartz tube ($2r_1 = 21.8$; $2r_0 = 24.8$ mm) in terms of an electron density is based on the calculations given in table I of ref. 2, and on the

calibration experiments described in section 5.1. For our case in which $r_1/r_0 = 0.88$ ($= a_{s-2}/a_{s-1}$ in ref. 2), we calculated for a closed cavity containing a quartz tube with a length equal to that of the cavity (ref. 2, fig. 3, $s = 3b$):

$$\langle f_p^2 \rangle = 4.05(f^2 - f_2^2), \tag{11}$$

where $f_p = \omega_p/2\pi$ is the plasma frequency, $f = \omega/2\pi$ is the resonance frequency of the cavity with tube and plasma, and f_2 is the resonance frequency of the cavity with empty quartz tube.

To apply this expression (11) in experimental circumstances in which an open cavity was mounted around a long discharge tube, the reduction factor $\gamma = 0.86$ was introduced (see 5.1). In addition we have the general relation: $f_p^2 = e^2 n_e (4\pi^2 m_e)^{-1} = 80.6 \, n_e$. Substitution of the latter relation in expression (11) and correcting by the factor γ gives:

$$\langle n_e \rangle = 5.84 \times 10^{-2}(f^2 - f_2^2). \tag{12}$$

For the discharge tube with $f_2 = 2830$ MHz this results in:

$$\langle n_e \rangle = 3.30 \times 10^8 \, \Delta f (1 + \Delta f/2f_2), \tag{13}$$

where the frequency shift Δf and the frequency f are given in MHz and $\langle n_e \rangle$ is measured in cm^{-3}.

The values of $\langle n_e \rangle$ found from expression (13) are given in section 6.

6. *Results: Comparison of n_e measurements.* Measurements with a microwave cavity, a microwave interferometer and Langmuir probes were performed in the discharge tube (discharge radius 11 mm) described in section 2.2. The tube current was varied between 20 mA and 150 mA; the helium-gas pressure from 0.15 torr up to 0.75 torr.

6.1. Comparison of the two microwave methods. In fig. 9 values of the measured cavity frequency shift (Δf) and the interferometer phase shift ($\Delta \phi$)† are given as a function of the tube current for different gas pressures. The measurements were performed simultaneously in the same discharge. The resulting curves are approximately straight in our measuring range, which means that the electron density is approximately proportional to the current density in this region. From the figure it is found that the ratio $\Delta \phi/\Delta f = 1.07 \pm 0.01$ degrees/MHz.

On the other hand the connection between the frequency shift and the phase shift can be derived from the calculations given in refs. 1 and 2. Ex-

---

† $\Delta \phi = (180/\pi) L(\beta_g - \beta)$ where L is the distance between the coupling holes, and β and β_g are, respectively, the propagation constant with and without a gas discharge in the tube.
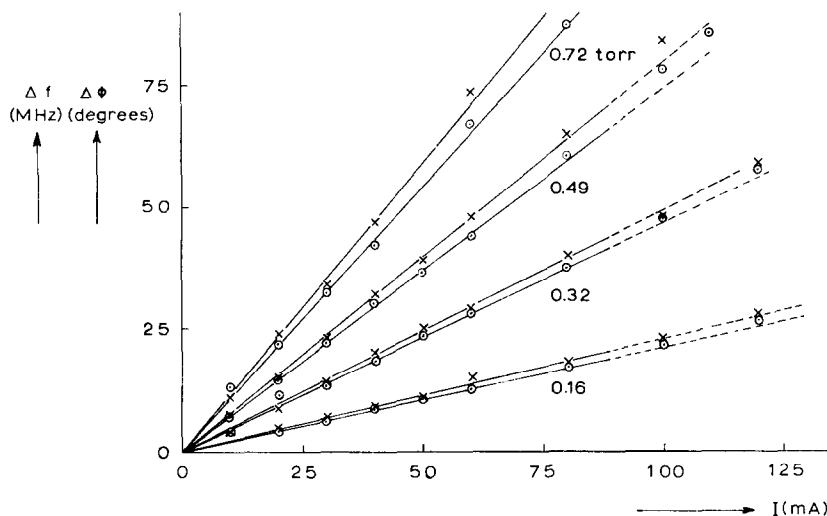
Fig. 9. The phase shift $\Delta\phi$ ($\times$) of the interferometer and the resonance shift Δf ($\circ$) of the cavity are given as a function of the tube current I with the pressure as a parameter. The measurements have been performed with $\beta_g = 135.8$ rad/m and $f = 2.832$ GHz. The mean value of the ratio $\Delta\phi/\Delta f = 1.07$ degrees/MHz.

pressions (10) and (13) give the relation between respectively the shift in the propagation constant β and the frequency shift and the mean electron density; however, the relations quoted are only valid in the range of small electron densities. In this case we derive:

$$3.15 \, \Delta\phi \text{ degrees} = \langle n_e \rangle \, 10^8 \text{ cm}^{-3} = 3.30 \, \Delta f \text{ MHz},$$

or

$$\Delta\phi/\Delta f = 1.05 \pm 0.01 \text{ degrees/MHz}.$$

Using the measured electron-density profiles instead of the parabola, the calculated value for $\Delta\phi/\Delta f$ increases to about 1.08 ± 0.02 degrees/MHz.

As the measured and the calculated ratios $\Delta\phi/\Delta f$ are the same within the estimated error we conclude that the microwave cavity calibrated with dielectric material ($\varepsilon > 1$, see section 5.1) can be used for measurements of electron densities in a discharge plasma ($\varepsilon < 1$).

6.2. Comparison of the probe method with microwave methods
The results of simultaneous measurements with the three devices (Langmuir probes, microwave cavity and microwave interferometer) are given in fig. 10 and table VI. The probe measurements of these series were performed with the "slow" method (X–Y recorder; the second derivative was measured too). Simultaneous measurements of the fast-probe method (oscillograph) and the microwave interferometer are given in the same figure. The fast method was used to avoid heating up of the probe at the higher electron
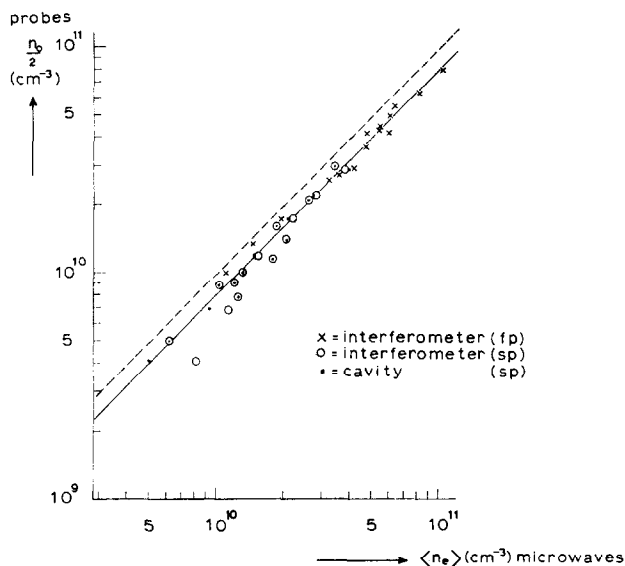
Fig. 10. Comparison of the average ($= \frac{1}{2}$ maximum) electron densities, measured by the probes and the two microwave devices. The lower electron densities have been measured with two microwave devices and the Langmuir probes simultaneously; the probe curves were plotted with the help of the X–Y recorder (slow recording of probe curves: sp). The higher electron densities have been measured only with the interferometer and the probes (with the fast registration method: fp). The difference with the dotted line, which would be found if the probe and microwave results were equal, is about 20%.

densities. In fig. 10 it is clearly demonstrated that there is an average difference between the probe and microwave results of about 20% for a parobolic profile, the probes being lower. If the measured profiles are used, the difference becomes 30%.

As follows from the results given in 6.1 there is a very good correlation between the results of the two microwave methods. This agreement gives a check on different steps; first of all the calculations given in refs. 1 and 2 are probably correct but there is another important fact, namely: the cavity calculations are nearly independent of the radial electron-density distribution but the interferometer is quite sensitive to the distribution which was also experimentally determined (see section 3.4).

The 30% difference between the electron densities measured with probes and microwaves as found experimentally may be explained for the greater part by secondary emission and reflection of electrons by the probe. A rough estimation (from experimental results on a clean platinum surface[13]) and on a tungsten surface[14]) leads to a correction of about 20% for the electron current to the probe if the electron temperature is 8 eV. Other corrections are concerned with secondary electrons freed by metastables

TABLE VI

Results of measurements

Discharge parameters			Cavity		Interferometer		Langmu
I	p	E	$\langle n_e \rangle$	μ_0	$\langle n_e \rangle$	μ_0	$\frac{1}{2}n(0)$
(mA)	(torr)	(V/cm)	(10^{10} cm^{-3})	(torr m^2/V s)	(10^{10} cm^{-3})	(torr m^2/V s)	(10^{10} cm^{-3}) (
80	0.20	3.9	0.61	99	0.62	97	0.50
80	0.30	4.1	1.03	85	1.03	85	0.88
80	0.41	4.2	1.43	81	1.56	75	1.18
80	0.49	4.2	1.84	76	1.87	75	1.60
80	0.67	4.3	2.62	71	2.63	71	2.12
80	0.20	3.8	0.48	129	0.72	86	0.41
80	0.25	4.1	0.91	80	1.10	67	0.59
80	0.33	4.1	1.22	79	1.24	78	0.93
80	0.50	4.2	2.08	69	2.05	69	1.40
150	0.20	3.8	1.28	91	1.28	91	1.00
150	0.32	3.9	2.11	87	2.18	84	1.75
150	0.36	4.0	2.69	82	2.82	79	2.25
150	0.48	4.0	3.37	79	3.42	78	2.95
150	0.20	3.8	1.27	93	1.23	96	0.78
150	0.25	3.8	1.77	83	1.78	83	1.15
150	0.50	4.0	4.02	70	3.81	74	2.85
150	0.67	4.1	—	—	4.73	77	4.10
80	0.32	4.2	—	—	1.11	81	0.98
80	0.50	4.2	—	—	1.92	74	1.75
100	0.32	4.1	—	—	1.44	82	1.35
200	0.32	3.8	—	—	3.18	79	2.60
200	0.50	3.9	—	—	5.33	72	4.50
300	0.33	3.7	—	—	5.32	75	4.35
300	0.50	3.8	—	—	8.14	72	6.25
390	0.33	3.8	—	—	6.29	81	5.50
400	0.50	3.8	—	—	1.00	79	8.00
364	0.33	3.8	—	—	6.00	79	4.00
300	0.23	3.6	—	—	3.54	80	2.75
380	0.23	3.6	—	—	4.14	81	2.95
400	0.23	3.5	—	—	4.77	81	3.70

(about 5%) and the fact that the electron distribution is other than :
wellian (also about 5%). As a consequence the 30% difference foun‹
tween the probe and microwave results is compensated, though the pɪ
numbers are difficult to calculate (see section 3.2.2).

From the above-mentioned results we conclude that in cases wher‹
values of the corrections are not accurately known, a calibration oɪ
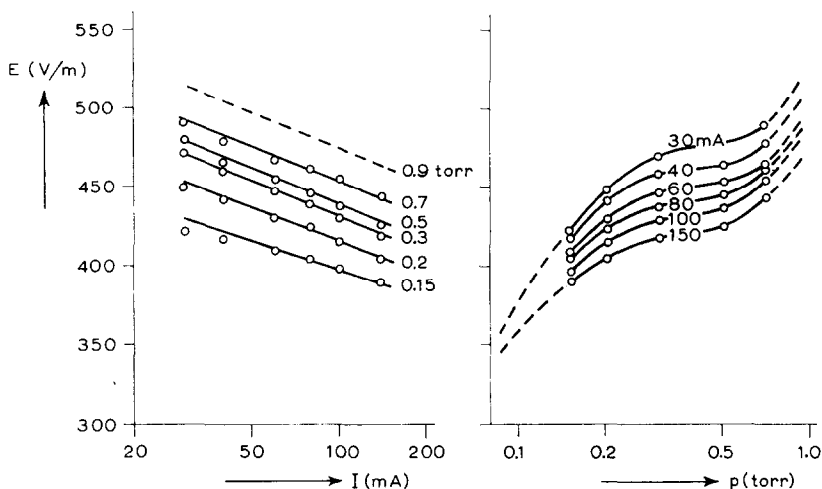probes with microwave methods may be appropriate.

Fig. 11. The axial potential gradient measured between two floating wall probes along the column of a stable discharge ($R = 11$ mm) in helium: a) as a function of the discharge current I; b) as a function of the gas pressure p.

7. *Results concerning the helium discharge.* 7.1. Potential gradients. To test the reproducibility and cleanliness of the discharge the potential difference was measured between two floating wall probes (1.5 mm diameter, separation 680 mm) as a function of tube current (30–150 mA) and gas pressure (0.1–1 torr). The measuring instrument was a Treubner static voltmeter; accuracy 2% of full scale. The results are given in the figs. 11a and 11b where the column voltage gradient E is given as a function of, respectively, the tube current I and the gas pressure p. Repeating the measurements on different days gives at most a difference of 5% in the values. The characteristic form of the curves, especially the inclination point at 0.3 torr is better reproducible; the curves shown in the figure were measured on one day. Decreasing values of E as a function of I have also been found by Klarfeld[18]) and should be attributed to the effect of stepwise ionization including metastables; see the calculations of Mewe[19]).

The increase in E as a function of p corresponds to the climbing branch of the Paschen curve. Extending the measurements to lower pressures a minimum in the voltage gradient was found at about 0.05 torr. (Here the tube imploded because of a hot spot on the glass in the cathode-fall region).

In fig. 12[†] our E/p values, given as a function of Rp ($R = 0.001$ m), are presented for two values of the tube current (0.03 and 0.15 A). Our values are compared with the results of Klarfeld[18]), Hoh and Lehnert[20]), Paulikas[21]) and Anderson[22]), because these investigators used about the same

---

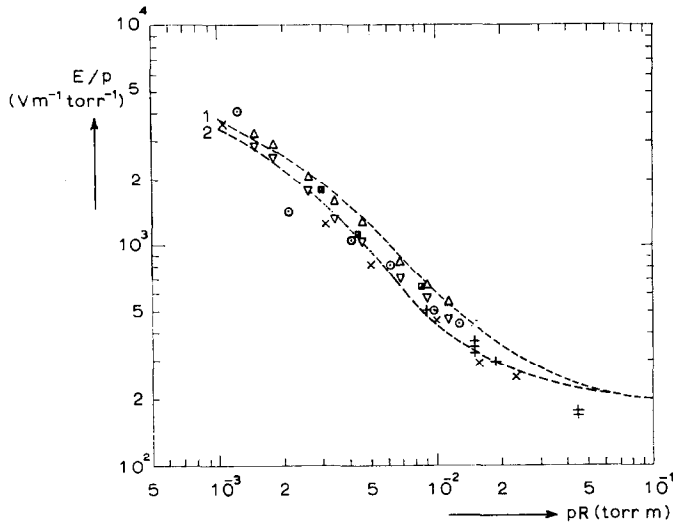† A presentation of the results in a form as given in fig. 12 is justified by theory.

Fig. 12. Comparison of experimental and theoretical data of E/p as a function of Rp.
Experimental and theoretical data:

	I	R	
△	0.03 A	0.011 m	Our results
▽	0.15	0.011	,, ,,
◪	0.01	0.0086	Anderson [22])
○	0.1	0.01	Hoh and Lehnert [20])
+	0.3	0.01	Klarfeld [18])
×	0.2	0.09	Paulikas [21])
1	0.01	0.1	Calculations by Mewe [19])
2	0.4	0.1	,, ,, ,,

current densities and tube radii as we did. As is shown in fig. 12 the results agree mutually within about 10%. A quantitative agreement between the values measured and calculations based on the results of theoretical considerations and measured concentrations of metastable atoms, has been found by Mewe [19]).

7.2. Electron densities. The average electron density $\langle n_e \rangle$ is a function of the helium-gas pressure p, the tube radius R, and the tube current I. In figs. 13a and 13b values of $\langle n_e \rangle$ are given as a function of I and p, respectively; they were measured with the microwave methods. Both functions are approximately linear except for the range $p < 0.1$ torr. To be able to compare these results with those of other authors we calculated the mobilities given in 7.3.

7.3. Electron mobilities. The electron mobility μ is defined in the following way: $v_d = \mu E$, where v_d is the drift velocity of the electrons. We
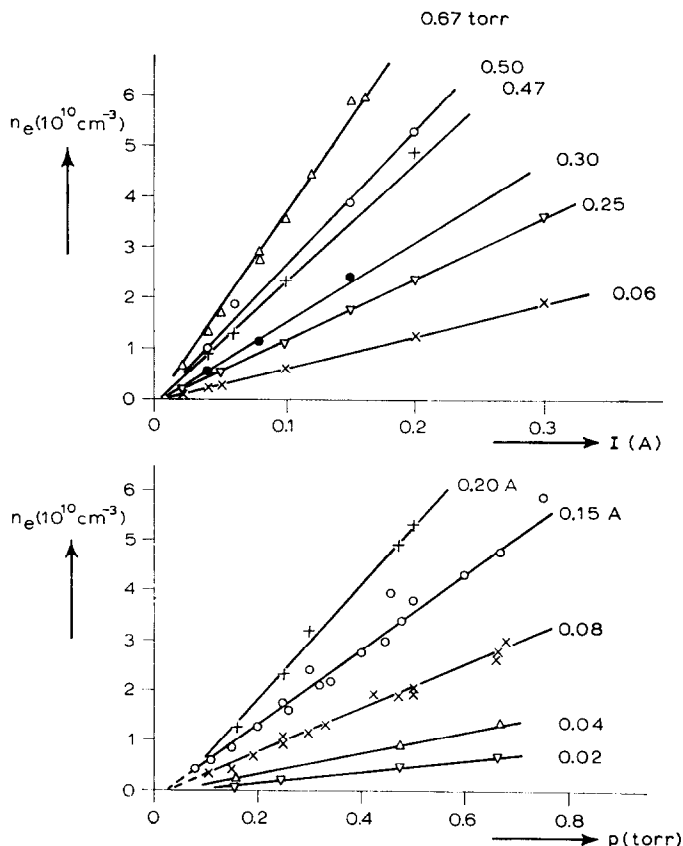
Fig. 13. The average electron density $\langle n_e \rangle$ measured through the aid of microwave methods in the positive column ($R = 11$ mm) of a discharge in helium: a) as a function of the discharge current I; b) as a function of the gas pressure p.

found v_d from the equality $I/\pi R_i^2 = \langle J_e \rangle = \langle n_e \rangle v_d e$ ($\langle J_e \rangle$ is the average value of the electron current density).

Values of μ_0, the electron mobility reduced to 1 torr and 0°C ($\mu_0 = \mu p_0 = \mu p \ 273/T$), are often given in the literature. The following expression is used:

$$\mu_0 = I p_0 (\pi R_i^2 \langle n_e \rangle \ eE)^{-1}, \tag{14}$$

where I is the tube current, p_0 the reduced gas pressure, R_i the radius of the discharge column and e the charge of the electron.

Values of μ_0 are given in figs. 14a and 14b as a function of I and p_0. It appears from fig. 14a that μ_0 does not depend on I; as a consequence the results in fig. 14b are given without using I as a parameter. Fig. 14b shows that the mobility depends on the pressure, decreasing at higher pressures.
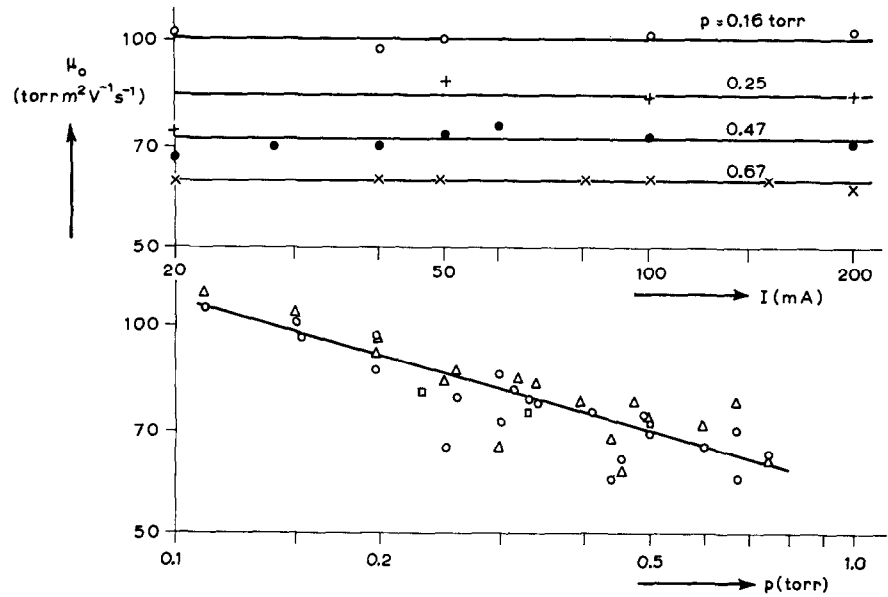
Fig. 14. The reduced electron mobility μ_0: a) as a function of the discharge current; b) as a function of the gas pressure (O = 80 mA, △ = 150 mA, □ = 300 mA).
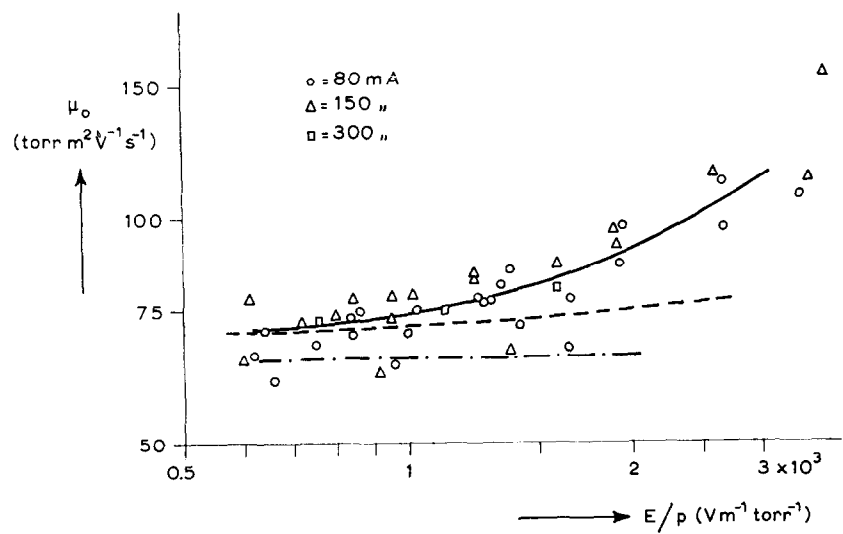

Fig. 15. The reduced electron mobility as a function of E/p calculated from our measurements at different discharge currents (————), compared with the results of Phelps[23] (————) and Anderson[22] (-.-.-).

From theoretical considerations one expects that μ_0 is a function of T_e and thus of E/p_0; in this form it is mostly given by other authors. Our results, calculated from the microwave measurements, are compared with mobilities calculated from the results of Phelps[23] and Anderson[22] in fig. 15. At low E/p values the agreement is quite satisfactory. At higher values of E/p our results increase in value, whereas the results of Phelps and Anderson are more or less constant. In their case the electron mean free path is much smaller than the tube radius. However, in our case these quantities are of the same magnitude for high E/p; as a consequence the electron orbit shape is more influenced by the radial electric field which may give an explanation for the difference.

APPENDIX I

1. *Determination of the dielectric constant.* The resonance frequency f of a uniformly filled closed cavity is given by

$$f = \frac{2.405}{2\pi\sqrt{\varepsilon}} \frac{c}{a} \text{ [ref. 2, expressions (16) and (4c)],} \tag{15}$$

where ε is the dielectric constant of the medium which fills the cavity, a the radius of the cavity, and c the velocity of light. After the substitution of $\varepsilon = 1$ and $a = 3.75 \times 10^{-2}$ m (the radius of our cavity) we calculated for the resonance frequency of the empty cavity used in our experiments: $f = 3060$ MHz. When this cavity was closed with metal seals a resonance frequency of $f = 3058 \pm 2$ MHz was measured, which satisfied us that the sealed-off cavity behaves in conformity which the calculations. With open end holes the resonance frequency is 3101 MHz, which indicates the disturbance of the electric field caused by the end holes.

Next we used the closed cavity for an accurate determination of the dielectric constants of different materials used in further experiments, at the working frequency (3 GHz) of the cavity. The volume, v, of the closed cavity was filled with small balls of polystyrene, having weight w, to find the dielectric constant of polystyrene. From experiments with massive and foamed balls we determined with the help of expression (15) that

$$(\varepsilon - 1)(v/w) = 1.073.$$

In the literature we find $\varepsilon = 2.0$–2.1 at this frequency and a specific weight of 0.98 from which follows: $1.02 < (\varepsilon - 1)(v/w) < 1.12$.

Furthermore we obtained dielectric constants from measurements on rods of dielectric material placed on the axis of the closed cavity. Using the calculation method given in ref. 2, eq. (21), the dielectric constant of the material was found from the shift in the resonance frequency caused by a rod of known diameter. In the experiments the values of the frequency

shifts were found directly by the difference of the resonance frequency with and without dielectric material. The results of these measurements are given in table VII.

2. *Determination of the ratio of the resonance frequencies with and without a quartz tube.* The resonance frequency of the closed cavity containing a quartz tube with diameters of 22 and 25 mm respectively and 50 mm length,

TABLE VII

Values of the dielectric constant of some materials obtained from measurements on rods in the closed cavity

Material	Diameter (mm)	Freq. shift (MHz)	ε
Teflon	4.76	23.9 ± 0.2	2.04 ± 0.02
,,	5.15	27.9 ± 0.2	2.04 ± 0.02
,,	12.2	148 ± 1	2.03 ± 0.02
,,	19.8	330 ± 1	2.02 ± 0.02
Parafine wax	12.4	187 ± 1	2.27 ± 0.02

was found on curve $S = 3b$ of fig. 3, ref. 2, where $\omega_{\mathrm{p}}^2 = 0$. The figure shows that for this situation $\omega^2/\omega_1^2 = 0.823$ and thus $f/f_1 = 0.907$.

From measurement we obtained for the open cavity $f/f_1 = 0.912$ in the same situation, in good agreement with the calculations.

REFERENCES

1) Kinderdijk, H. M. J. and Hagebeuk, H. J. L., Physica 52 (1971) 229.
2) Van Eck, J. and Kinderdijk, H. M. J., Physica 52 (1971) 316.
3) Schulz, G. J. and Phelps, A. V., Rev. sci. Instrum. 28 (1957) 1054.
4) Luijendijk, S. C. M. and Van Eck, J., Physica 36 (1967) 49.
5) Langmuir – Collected Works, Vol. 4, p. 23, Pergamon Press (N.Y., 1961).
6) Postma, A. J., Physica 45 (1970) 609 and 43 (1969) 581.

7) Medicus, G., J. appl. Phys. **32** (1961) 2512 and **33** (1962) 3094.
8) Kagan, Yu. M. and Perel, V. I., Soviet Physics – Uspekhi (1964) p. 767.
9) Laframboise, J. G., UTIAS Report No 100, Toronto, Canada, 1966.
10) Freudenthal, J. and Kinderdijk, H. M. J., Physica **32** (1966) 158.
11) Mewe, R., Physica **47** (1970) 373.
12) Dorrestein, R., Aansl. Functies van Metastabiele Toestanden, thesis, Utrecht 1941.
13) Hölzl, J., Z. Phys. **184** (1965) 50.
14) Ahearn, A. J., Phys. Rev. **38** (1931) 1857.
15) Verwey, W., thesis, Utrecht 1960.
16) Van Eck, J. and Kinderdijk, H. M. J., 8 Int. Conf. Phen. Ion. Gases, Vienna (1967) 483.
17) Thomassen, K. I., J. appl. Phys. **34** (1963) 1622.
18) Klarfeld, B. N., J. Phys. USSR **5** (1941) 155.
19) Mewe, R., Rijnhuizen Report 70 – 58 (1970).
20) Hoh, F. C. and Lehnert, B., Phys. Fluids **3** (1960) 600.
21) Paulikas, G. A., UCRL 9588 (1961).
22) Anderson, J. M., Phys. Fluids **7** (1969) 1517.
23) Phelps, A. V. and Pack, J. L., Phys. Rev. **117** (1960) 470.